Motor-driven marginal band coiling promotes cell shape change during platelet activation

Boubou Diagouraga,[1] Alexei Grichine,[1] Arnold Fertin,[2] Jin Wang,[3] Saadi Khochbin,[1] and Karin Sadoul[1]

[1]Institut Albert Bonniot, Institut National de la Santé et de la Recherche Médicale U823; and [2]Techniques de l'Ingénierie Médicale et de la Complexité–Informatique, Mathématiques et Applications, Grenoble, Centre National de la Recherche Scientifique Unité Mixte de Recherche 5525; Université Joseph Fourier–Grenoble 1, F-38041 Grenoble, France
[3]State Key Laboratory of Medical Genomics, Department of Hematology, Shanghai Institute of Hematology, Ruijin Hospital, Shanghai Jiao Tong University School of Medicine, Shanghai 200025, China

Platelets float in the blood as discoid particles. Their shape is maintained by microtubules organized in a ring structure, the so-called marginal band (MB), in the periphery of resting platelets. Platelets are activated after vessel injury and undergo a major shape change known as disc to sphere transition. It has been suggested that actomyosin tension induces the contraction of the MB to a smaller ring. In this paper, we show that antagonistic microtubule motors keep the MB in its resting state. During platelet activation, dynein slides microtubules apart, leading to MB extension rather than contraction. The MB then starts to coil, thereby inducing the spherical shape of activating platelets. Newly polymerizing microtubules within the coiled MB will then take a new path to form the smaller microtubule ring, in concerted action with actomyosin tension. These results present a new view of the platelet activation mechanism and reveal principal mechanistic features underlying cellular shape changes.

Introduction

Mammalian platelets are small cell fragments with neither nucleus nor microtubule organizing center. They circulate in the blood stream to survey vascular integrity. In their quiescent state, they have a flat, discoid morphology caused by a microtubular ring structure, called the marginal band (MB), in the periphery of resting platelets (White and Rao, 1998). Endothelial damage will induce platelet activation, which is composed of several successive events (Hartwig, 2006). Within seconds, they adopt a 3D, sphere-shaped morphology, extend filopodia, secrete the content of their granules, and spread on the subendothelial layer or aggregate with surrounding platelets to form a hemostatic plug. In the activated platelet, a smaller microtubule ring structure is observed, and it has been suggested that actomyosin tension leads to the spherical shape and induces the centripetal contraction of the MB (White and Burris, 1984; Johnson et al., 2007). So far, microtubule motor proteins have not been implicated in the maintenance of the resting MB, the shape change, or the MB reorganization during platelet activation (Patel et al., 2005; Hartwig, 2006).

MB microtubules in resting platelets are heavily acetylated (Patel-Hett et al., 2008). In general, prominent microtubule acetylation is observed when microtubule motor actions are important either for cellular transport processes (Reed et al., 2006; Dompierre et al., 2007) or for microtubule movements, as for instance, in mitotic spindles, primary cilia, or flagella (Piperno et al., 1987; Schatten et al., 1988). We therefore hypothesized that microtubule motor proteins might be functionally important in platelets.

Results and discussion

Microtubule motor actions in platelets

To investigate whether microtubule motors could play a functional role in platelets, we first performed Western blotting to test for their presence in platelet lysates using pan-anti–kinesin heavy chain and dynein intermediate chain antibodies. Kinesin heavy chains of 68 and 72 kD as well as the dynein intermediate chain of 74 kD were detected in platelet lysates (Fig. 1 A) as described previously (Rothwell and Calvert, 1997; Patel et al., 2005). We then treated resting platelets with the dynein inhibitor erythro-9-[3-2-(hydroxynonyl)]adenine (EHNA; Penningroth et al., 1982) and either fixed them in suspension (resting state)

Saadi Khochbin and Karin Sadoul contributed equally to this paper.
Correspondence to Karin Sadoul: karin.sadoul@ujf-grenoble.fr

Abbreviations used in this paper: ATA, aurintricarboxylic acid; EHNA, erythro-9-[3-2-(hydroxynonyl)]adenine; MB, marginal band; PRP, platelet-rich plasma.

The Rockefeller University Press $30.00
J. Cell Biol. Vol. 204 No. 2 177–185
www.jcb.org/cgi/doi/10.1083/jcb.201306085

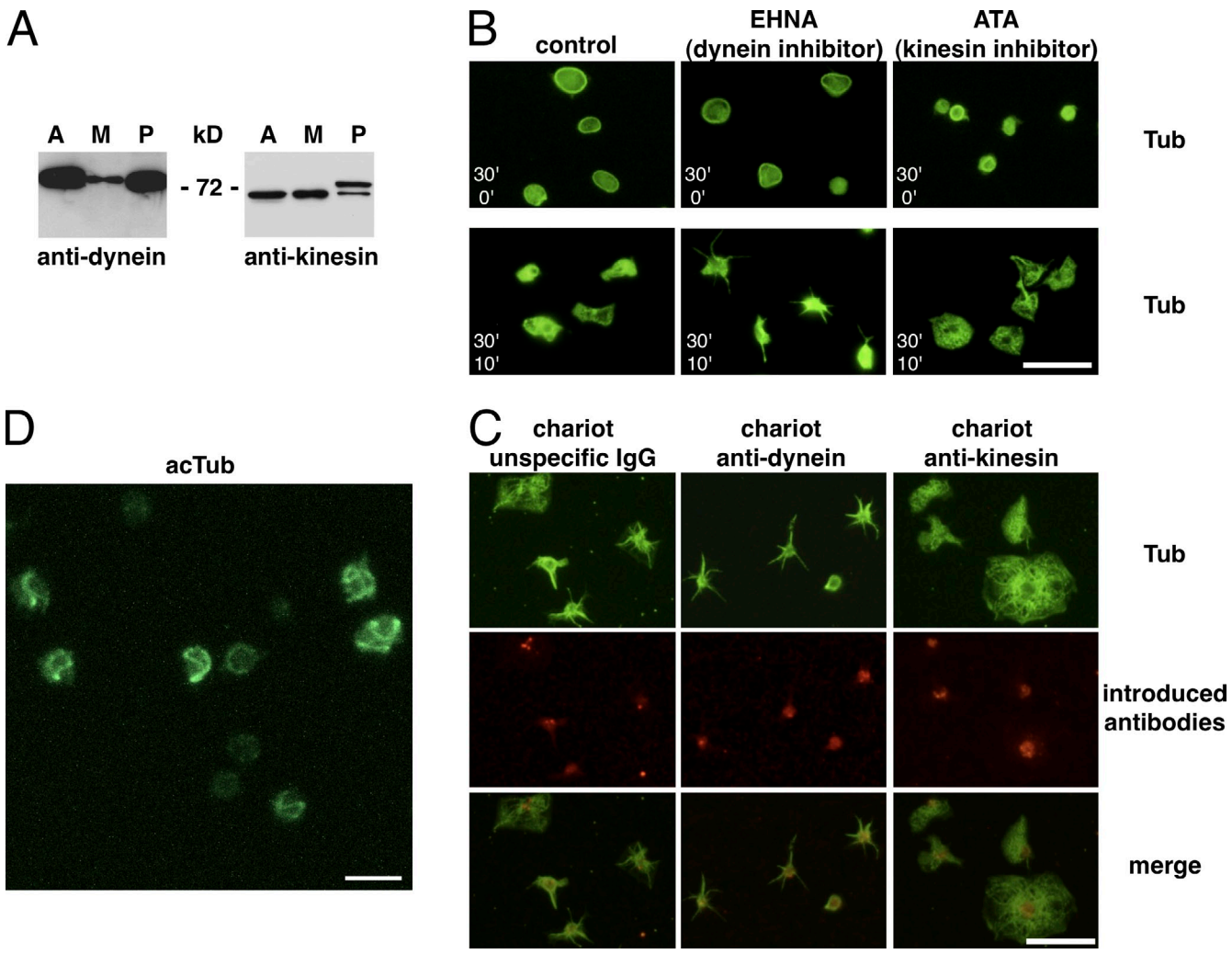

Figure 1. **Presence of microtubule motors in platelets and motor inhibitor treatments.** (A) Western blot of 5 µg lysates of the cell line A549 (A), the megakaryocyte precursor line CHRF-288-11 (M), and of 10^7 platelets (P) revealed with a pan-anti–kinesin heavy chain and an anti–dynein intermediate chain antibody. (B) Resting platelets in PRP from buffy coats were diluted in PBS, 2.5 × 10^6/ml, and incubated with 1 mM EHNA or 10 µM ATA for 30 min at RT and then either fixed (top; 30′ inhibitors/0′ spreading) or allowed to spread on a glass surface for 10 min (bottom; 30′ inhibitors/10′ spreading) before fixation and α-tubulin staining. (C) Control rabbit IgGs as well as mouse anti-dynein and rabbit anti-kinesin function-blocking antibodies were introduced into living platelets using the Chariot kit. Platelets were then allowed to spread on glass coverslips for 10 min, fixed, and stained using a monoclonal rabbit anti α-tubulin antibody for the anti-dynein Chariot and a mouse anti–α-tubulin antibody for the control and the anti-kinesin Chariot conditions (in green) as well as secondary antibodies recognizing the introduced antibodies (anti–mouse for the dynein Chariot and anti–rabbit for the control and the kinesin Chariot conditions, in red). (D) 3D projection of a confocal z stack of platelets treated as in B (top) with 10 µM ATA but for only 3 min, fixed, and stained for acetylated tubulin (acTub). Video 1. Bars: (B and C) 10 µm; (D) 5 µm.

or centrifuged them onto glass coverslips to let them spread for 10 min at 37°C as a test for their activation capacity. No obvious alteration of resting platelets is observed after dynein inhibition, whereas spreading is almost completely prevented. Surprisingly, use of the kinesin inhibitor aurintricarboxylic acid (ATA; Duhl and Renhowe, 2005) in the same assay, results in a smaller microtubule ring in resting platelets, but platelets are still able to spread on a glass surface and do so with a more round morphology (Fig. 1 B and Fig. S1, A and B, for quantification).

These inhibitor experiments suggested that both microtubule motors have a functional role in platelets. To confirm these results, we introduced the kinesin and dynein antibodies, previously shown to be function blocking (Theiss et al., 2005; Grabham et al., 2007), into resting platelets using the Chariot kit. Dynein antibodies inhibited platelet spreading, resulting in the appearance of a majority of star-shaped platelets, similar to EHNA treatments. After introduction of kinesin antibodies, platelets were able to spread, and a higher number of fully round, spread platelets was observed, again similar to treatments with ATA (Fig. 1 C and Fig. S1 B, for quantification).

MBs coil during platelet activation

Activated platelets have smaller microtubule rings than nonactivated platelets, and it has been suggested that this is caused by MB contraction (White and Burris, 1984). Because kinesin inhibition leads to a smaller microtubule ring (Fig. 1 B, top), we wondered whether kinesin inhibition could trigger MB contraction. Thus, platelets were treated with ATA for a shorter time period (3 min), fixed in suspension, and stained for tubulin (not depicted) or acetylated tubulin (Fig. 1 D). Half of the platelets

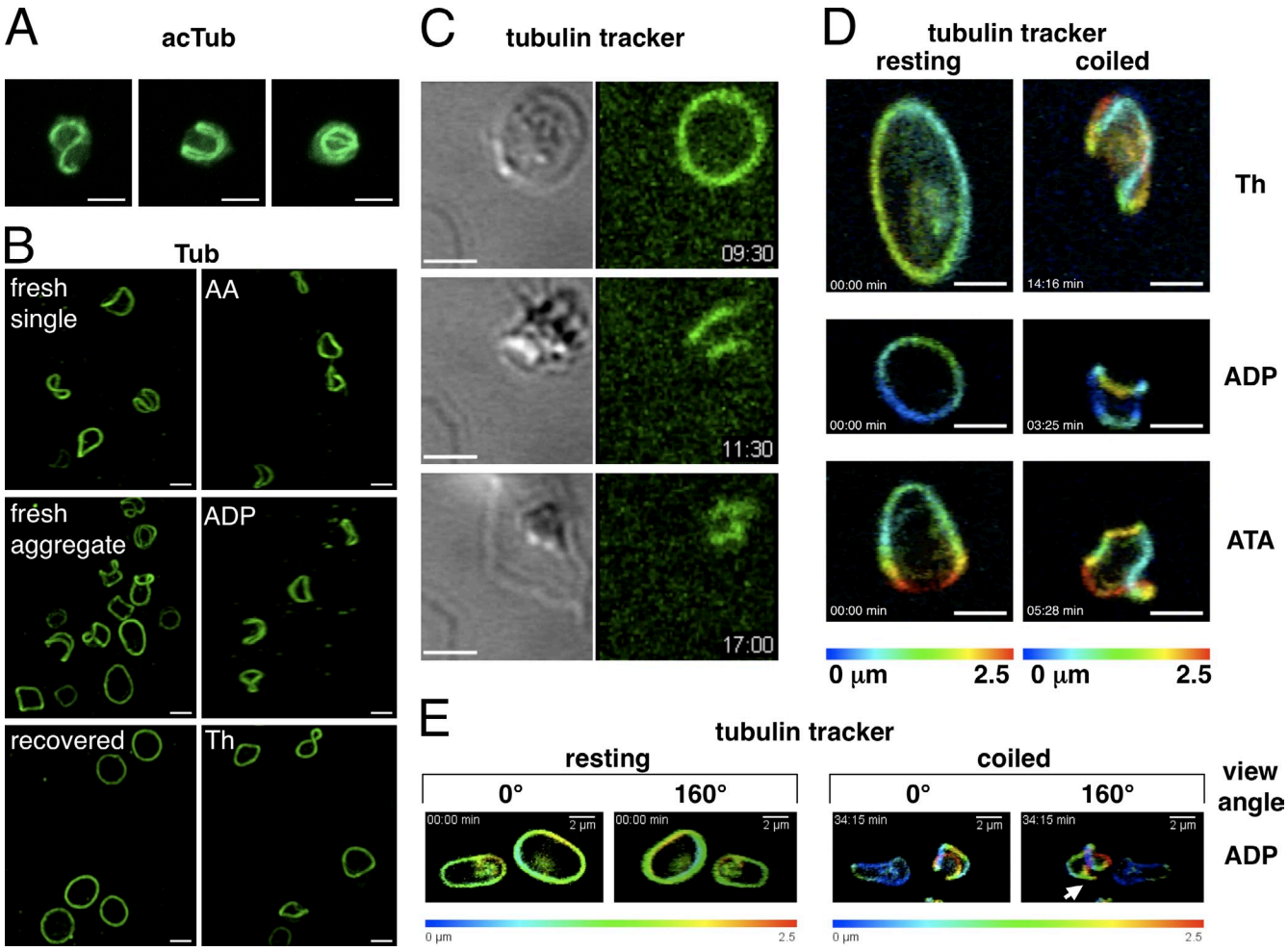

Figure 2. **MB coiling in activating platelets.** (A) 3D reconstruction of confocal z stacks of three representative examples of transiently activated platelets present in PRP prepared from freshly drawn blood, fixed, and stained for acetylated tubulin (AcTub). Video 2. (B, left images) Transiently activated platelets present in PRP prepared from freshly drawn blood: either single platelets, platelets forming a small aggregate, or platelets of the same PRP, which have regained the resting state after a recovery period (120 min at RT). (right images) Platelets present in PRP prepared from buffy coats activated for 60 s with the following agonists: 6.25 µM arachidonic acid (AA), 25 nM ADP, and 0.01 U/ml thrombin (Th). Platelets are stained for α-tubulin. Video 3. (C) Time-lapse video of a microtubule tracker-stained platelet spreading on a glass surface. Transmission (left) and fluorescence (right) images are taken simultaneously every 5 s. Three time points of the activation sequence are shown: disc shape with resting MB, sphere shape with coiled MB, and spread platelet with small microtubule ring. Video 4. Time points are given in minutes and seconds. (D) Two time points of time-lapse videos of 3D reconstructions of confocal stacks of microtubule tracker-stained platelets activated with thrombin (0.017-U/ml final) and ADP (135-nM final) or treated with ATA (6.7-µM final). 3D projections are depth color coded as indicated. Video 5. (E) Two time points of a time-lapse video of 3D reconstructions of confocal stacks of microtubule tracker-stained platelets activated with ADP (270-nM final). 3D projections are depth color coded as indicated. Shown are two different view angles to observe microtubules short cutting the coiled bundle (arrow). Video 6. Bars, 2 µm.

(48.4 ± 6.1%) still had the characteristic flat MB of resting platelets, and 22.8 ± 5.5% had a smaller ring. To our surprise, we observed in the remaining 28.8 ± 8.3% a 3D twist of the MB (four independent experiments). Platelets with coiled MBs had lost their disc shape and were more spherical. Thus, MB coiling induced by kinesin inhibition results in a disc to sphere transition and ultimately in a smaller microtubule ring structure, two hallmarks of activating platelets. We thus wondered whether MB coiling is the molecular mechanism leading to sphere shape during platelet activation. If so, it should be possible to detect MB coiling under physiological conditions.

Immediately after, venipuncture platelets are in a reversible activated state as a consequence of the mechanical stress (Lippi et al., 2013). In platelet populations prepared directly after blood sampling and stained for tubulin and acetylated tubulin (Fig. 2, A and B; and Videos 2 and 3), only 32 ± 12.6% were in the resting state, whereas the majority had a spherical shape with twisted MBs (68.2 ± 12.6%, seven independent experiments using blood from three different donors), reinforcing the idea that MB coiling induces sphere shape. After a recovery period of ∼2 h at RT, platelets had regained their flat disc shape and a normal MB (Fig. 2 B and Video 3). MB coiling was also observed when resting platelets in suspension were activated for 60 s with low concentrations of different agonists (Fig. 2 B and Video 3), whereas concentrations used in standard aggregation assays resulted in the smaller microtubule ring (not depicted).

Furthermore, MB coiling is also observed during spreading of living microtubule tracker-stained platelets on a glass surface (Fig. 2 C and Video 4). The fluorescent image of the time-lapse video shows that the MB started to coil (at a time

point of 9 min and 50 s) when the transmission image shows the beginning of disc to sphere transition (at 10 min and 20 s, sphere shape is reached). We also used time-lapse video microscopy to follow platelet activation in suspension triggered with different agonists and observed MB coiling under all conditions tested (Fig. 2, D and E; and Videos 5 and 6).

Thus, MB coiling induces sphere shape and is part of the sequence of events leading to platelet activation. Although it has long been recognized that the MB is essential to keep the discoid shape of resting platelets (White and Rao, 1998), this is the first description of MB coiling inducing the rapid disc to sphere transition of activating platelets, first described in 1965 (Bull and Zucker, 1965). Interestingly, highly similar microtubule coils have been described in limulus amebocytes and nucleated thrombocytes of nonmammalian vertebrates, indicating that this process is evolutionarily conserved (Conrad et al., 2004; Lee et al., 2004).

Dynein is implicated in MB coiling

One possible reason for MB coiling could be the limited available space either after actomyosin contraction or after MB extension. In favor of the latter hypothesis is the finding that MB length measurements after 3D reconstructions of confocal image stacks show that coiling MBs in freshly prepared platelets are statistically longer compared with flat MBs in resting platelets (Fig. 3 A). MB extension could be caused by dynein-induced sliding apart of microtubules similar to the dynein-mediated microtubule-sliding process responsible for proplatelet extension in megakaryocytes (Patel et al., 2005). Such a mechanism is supported by our observation that transiently activated platelets with coiled MBs present in freshly drawn blood rapidly get back to their resting discoid shape upon dynein inhibition (27.3 ± 10.7% resting platelets in control vs. 67.2 ± 13% in EHNA-treated populations; five independent experiments, $P < 0.01$; Fig. 3 B). Furthermore, we observed that EHNA treatment inhibits MB coiling induced by platelet activation with ADP (Fig. S2 A).

However, although MB extension may be sufficient to induce MB coiling, it is not essential. Coiling is also observed when microtubule motor actions are bypassed by directly activating actomyosin contraction with calyculin (Fig. S2 B and Video 10). MB length measurements using the tracker films also show that MBs can coil without significantly elongating (Fig. S3). This may be attributed to the tracker stain in this case because it has an unexpected effect on platelets. Platelets stained with the taxol-based tracker kit have enhanced activation responses to ADP, whereas taxol-treated platelets have reduced responses (Fig. S2 A). One possible explanation for this result could be that the surfactant component of the tracker stain destabilizes actomyosin/microtubule connections, which may facilitate actomyosin contraction and bypass microtubule motor actions. Although our results demonstrate that MBs coil during platelet activation, they do not explain how the smaller ring structure observed in activated platelets might form.

Newly polymerizing microtubules form the smaller ring after actomyosin contraction

To investigate the formation of the smaller ring structure, we based our strategy on the pioneering work by Patel-Hett et al. (2008). They have shown that the MB is composed of stable and several actively polymerizing microtubules and that it can be stained with antibodies against acetylated and tyrosinated α-tubulin. Tyrosinated α-tubulin constitutes the pool of free tubulin subunits used by newly polymerizing microtubules (Janke and Bulinski, 2011). To visualize simultaneously stable/acetylated, newly formed/tyrosinated, and total microtubules, we acquired confocal images of triple-stained platelets with MBs at different coiling stages. 3D reconstructions of individual stainings and merges are shown, and to better appreciate colocalizations, images were thresholded, and MBs were skeletonized. All three stainings colocalize in resting platelets and in platelets with slightly coiled MBs (Fig. 4, A–C; and Video 8). In contrast, in platelets with strongly coiled MBs, newly formed microtubules take a new path by switching to the proximal part of the microtubule bundle, which leads to the formation of a smaller ring (Fig. 4, D–F; and Video 9). The coiling stage when microtubules just start to use a new path (Fig. 4 C) reaching for the opposite side of the coiled bundle is also illustrated in Video 6 associated with Fig. 2 E (arrow).

The more the coiled MB appears compressed, the smaller is the new ring and actomyosin contraction may come into play at this point. To test this, we treated resting platelets with the myosin inhibitor blebbistatin, shown previously to block actomyosin contraction in platelets (Calaminus et al., 2007; Johnson et al., 2007) or used cytochalasin D to depolymerize the actin cytoskeleton. As expected, blebbistatin and cytochalasin D had no influence on the resting MB, and platelet activation by ADP leads to the smaller microtubule ring in control platelets. This process requires an intact actin cortex because pretreatment with cytochalasin D prevents the smaller ring formation. At a blebbistatin concentration of 25 µM, the smaller ring appears slightly larger compared with the control. Similar results using blebbistatin and cytochalasin pretreatment before thrombin-induced platelet activation have been obtained previously (Severin et al., 2013). This has been interpreted as a requirement of actomyosin actions for the centripetal contraction of the MB to a smaller ring. However, careful examination of confocal image stacks reveals the presence of several platelets with coiled MBs, which is more evident when a blebbistatin concentration of 50 µM was used (47.4 ± 5.2%; Fig. 5 A). Thus, actomyosin contraction is required to compress the coiled MB, and its efficiency may decide about the fate of activating platelets. In the case of sustained actomyosin contraction, platelets may proceed to full, irreversible activation, and microtubules, polymerizing along the coiled, compressed MB, will form the smaller ring structure. In transiently activated platelets, actomyosin contraction is not maintained, and the new path taken by actively polymerizing microtubules will attain the size of a resting MB, which leads to platelets having simultaneously a coiled/elongated and a flat/resting MB (Fig. 4 D). Such platelets have been described previously by Behnke and Forer (1998). They can be found sporadically in populations of resting platelets (1–5%; not depicted) and more importantly in platelet populations prepared from freshly drawn blood after dynein inhibition, when they come back to the resting state (Fig. 3 B, arrows). The flat, newly polymerized MB may be progressively reacetylated, whereas the coiled, acetylated bundle, no longer used by newly

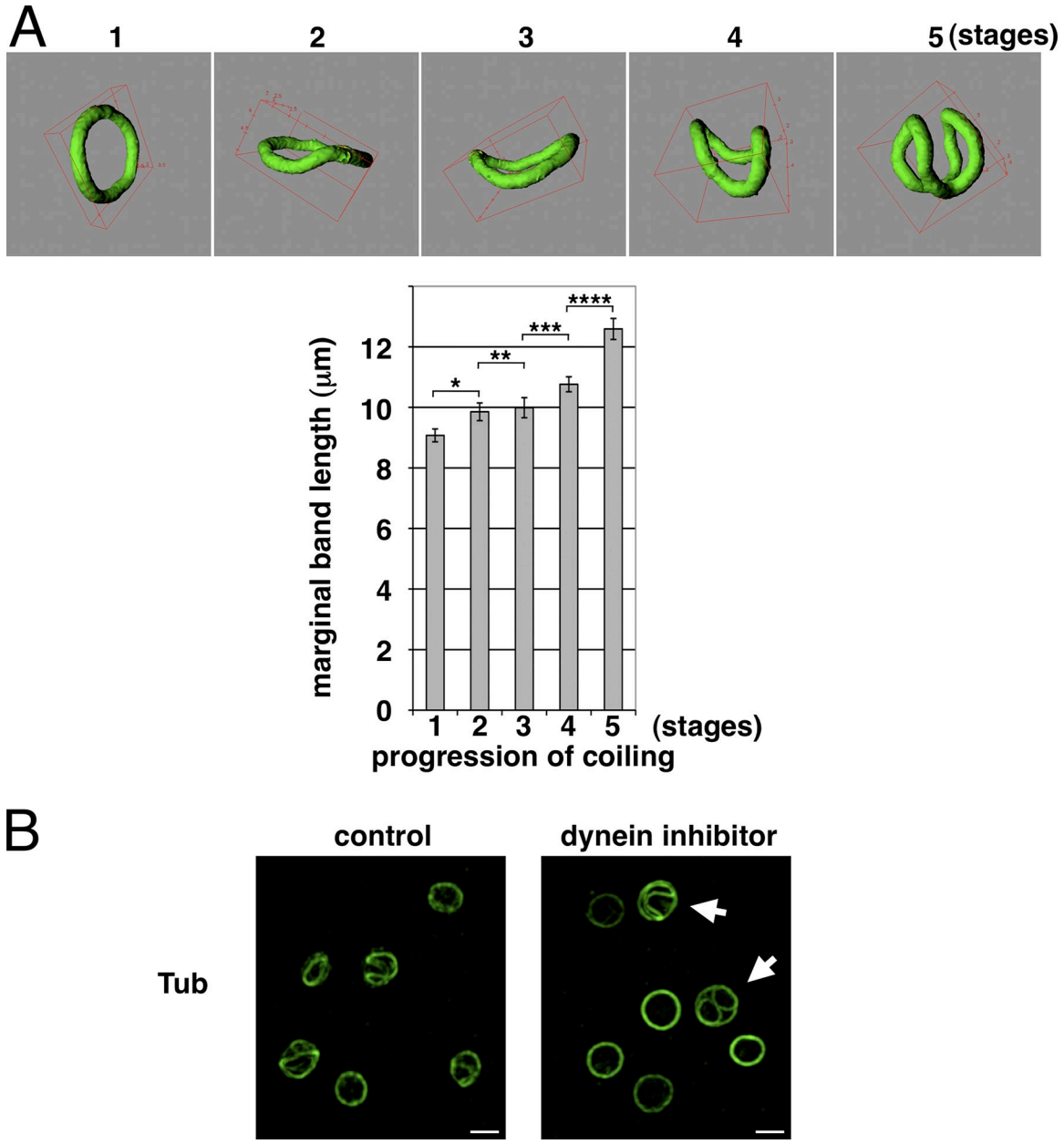

Figure 3. **Dynein-mediated MB extension induces its coiling.** (A) The MB length of resting platelets (PRP prepared from freshly drawn blood after a recovery period) and transiently activated platelets, present in PRP prepared from freshly drawn blood, was measured as described in the Materials and methods section. Platelets were grouped in five categories according to different coiling stages (stage 1, resting platelets, $n = 66$; stage 2, start of coiling, $n = 31$; stage 3, slightly coiled, $n = 32$; stage 4, more coiled, $n = 33$; and stage 5, maximum coiled, $n = 16$; data are presented as means ± SEM; *, $P < 0.017$; **, $P < 0.38$; ***, $P < 0.033$; ****, $P < 0.0009$). (B) Platelets prepared from freshly drawn blood with coiling MBs were diluted in PBS, 2.5×10^6/ml, and incubated with or without EHNA (1-mM final) for 10 min at RT, fixed, and stained for α-tubulin (Tub). Arrows indicate platelets having simultaneously coiled and resting MBs. Video 7. Bars, 2 µm.

polymerizing microtubules, might be rapidly depolymerized and deacetylated. This could explain the high degree of heterogeneity of MB acetylation in resting platelets. A low acetylation level may be indicative of a recent transient activation event. The rapid tubulin deacetylation observed during platelet activation (Sadoul et al., 2012; Aslan et al., 2013) may also depend on the depolymerization of the coiled part of the MB to give the deacetylase HDAC6 access to its preferred substrate, unpolymerized tubulin (Matsuyama et al., 2002). Dynein-induced MB coiling takes place when microtubules are acetylated (Fig. 1 D and Fig. 2 A). Like for dynein-mediated cargo transport (Dompierre et al., 2007), acetylation may enhance dynein actions, which could speed up coiling and explain the faster spreading capacity of platelets with hyperacetylated MBs (Sadoul et al., 2012).

The combined results allow us to deduce a putative model (Fig. 5 B) to explain the cross talk between the actin and tubulin part of the cytoskeleton, previously shown to be also important for platelet size determination (Thon et al., 2012). The absolute requirement of an intact actin cytoskeleton for MB coiling may suggest that it serves as support for dynein-mediated microtubule

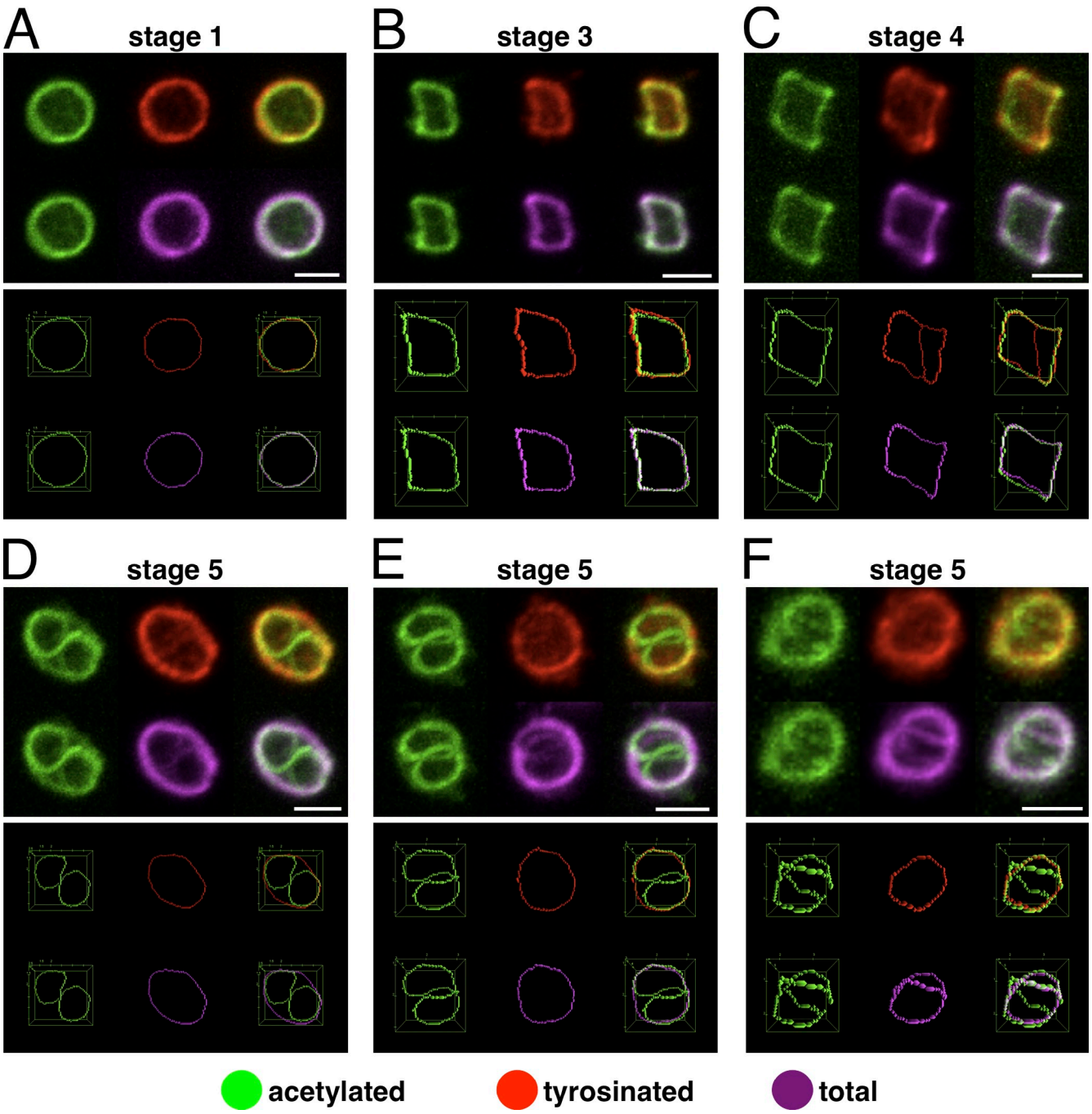

Figure 4. **Newly polymerizing microtubules form a smaller microtubule ring in activated platelets.** (A–F) Platelets with MBs at different coiling stages were triple immunostained for acetylated α-tubulin, tyrosinated α-tubulin, and total α-tubulin. Individual stainings as well as merges of 3D reconstructions of confocal z stacks are shown in the top images. The bottom images are generated from the different stainings after thresholding and skeletonizing of the MBs. For further details, see the legends of Videos 8 and 9. Bars, 2 µm.

sliding. Similar to nucleated cells (Tolić-Nørrelykke, 2008; Laan et al., 2012), dynein may be anchored to the actin cortex and slide microtubules apart once an activation signal reduces kinesin counteractions. Elongation of the MB then leads to its coiling, which might tear on (or rupture) microtubule–cortex interactions. This could be sensed by actomyosin as a signal to contract and compress the coiled MB.

In conclusion, this study sheds a completely new light on the events leading to platelet activation. The information that microtubule motor actions play a role in platelet physiology and are possibly regulated by microtubule acetylation highlights new directions for the development of therapeutic strategies able to modify platelet function. Furthermore, this study investigates cytoskeletal elements in a physiological cellular context in the absence of the nucleus and centrosomes. It reveals a tight interplay between the actomyosin and the microtubule part of the cytoskeleton governing rapid cell shape changes.

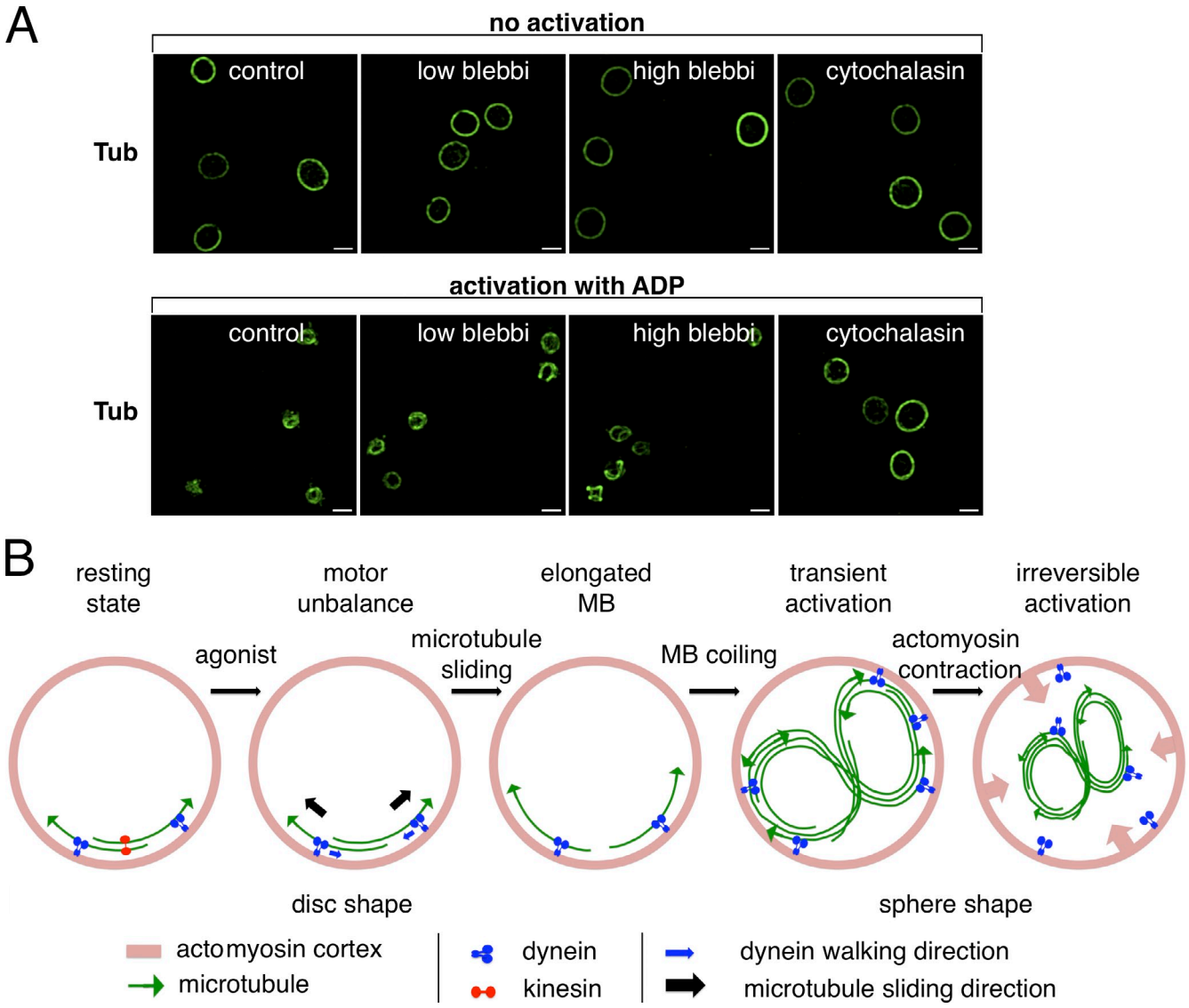

Figure 5. **Actomyosin contraction compresses the coiled MB.** (A) Platelets were diluted in PBS, 2.5 × 10^6/ml, and pretreated with or without 25 or 50 µM blebbistatin (blebbi) or 1 µg/ml cytochalasin D for 30 min at RT. Platelets were then either activated with ADP (2.5-µM final) for 10 min at RT (bottom) or not activated (top), fixed, and stained for α-tubulin. Bars, 2 µm. (B) Putative sequence of events leading to platelet activation (to simplify, only two microtubules are shown in disc-shaped platelets).

Materials and methods

Reagents and antibodies

The following antibodies were used: mouse anti–acetylated tubulin (clone 6-11B-1; T6793; Sigma-Aldrich), mouse anti–α-tubulin (clone B-5-1-2; T5168; Sigma-Aldrich), monoclonal rabbit anti–α-tubulin (clone EP1332Y; 04–1117; EMD Millipore), monoclonal rat anti–tyrosinated α-tubulin (gift of A. Andrieux, Grenoble Institut des Neurosciences, Grenoble, France), rabbit anti–kinesin heavy chain (AKINO1; Cytoskeleton, Inc.), mouse anti–dynein intermediate chain (clone 74.1; MAB1618; EMD Millipore), non-immune rabbit IgGs (I5006; Sigma-Aldrich), Alexa Fluor 488 goat anti–mouse IgG (A11029; Invitrogen), Alexa Fluor 488 goat anti–rabbit IgG (A11034; Invitrogen), Alexa Fluor 546 goat anti–mouse IgG (A11030; Invitrogen), Alexa Fluor 546 goat anti–rabbit IgG (A11035; Invitrogen), Alexa Fluor 546 goat anti–rat IgG (A11081; Invitrogen), Alexa Fluor 647 goat anti–rabbit IgG (A21245; Invitrogen), HRP goat anti–rabbit IgG (P0448; Dako), and HRP goat anti–mouse IgG (P0447; Dako). The following reagents were used: phalloidin-rhodamine (Sigma-Aldrich), Tubulin Tracker (Invitrogen), cytochalasin D (Sigma-Aldrich), poly-D-lysine (Sigma-Aldrich), thrombin (Sigma-Aldrich), arachidonic acid (Helena Biosciences), and ADP (Helena Biosciences).

Cell culture

The human lung carcinoma cell line A549 and the human megakaryocytic cell line CHRF-288-11 were cultured in RPMI 1640/10% FCS.

Preparation of human platelet-rich plasma (PRP)

Nontherapeutic buffy coats were diluted with an equal volume of PBS and centrifuged for 10 min, 400 *g*, at RT, and the upper phase corresponding to the PRP was collected. Alternatively, PRP from freshly drawn citrated blood (needle Eclipse [BD]; Vacutainer [BD]) was prepared identically but without prior PBS dilution.

Detection of microtubule motor proteins in cell lysates

A549 cells, megakaryocyte precursor cells (CHRF-288-11), and platelets prepared from buffy coats were lysed in sample buffer for SDS-PAGE and boiled for 5 min. Samples were run on a 10% gel and transferred onto polyvinylidene difluoride membranes. Motor protein subunits were revealed with a pan-anti–kinesin heavy chain and an anti–dynein intermediate chain antibody.

Spreading assay

Platelets are diluted in PBS and pipetted into 24-well plates with coverslips (10^6/400 µl/well). Plates are then centrifuged for 3 min, 600 *g*, at RT to assure simultaneous platelet contact with glass surfaces, allowing synchronized

spreading. Platelets are fixed in 4% neutral formalin after the indicated spreading times. For the resting state, platelets are first fixed and then pipetted into 24-well plates with glass coverslips (coated with 0.02 mg/ml poly-D-lysine for 1 h at RT) and centrifuged for 5 min, 600 *g*, at RT.

Motor inhibitor treatments

For kinesin inhibition, platelets were diluted in PBS to a concentration of 2.5×10^6/ml and then incubated with freshly prepared ATA (Sigma-Aldrich) at a final concentration of 10 µM for initial experiments and at 40 µM for quantification experiments to account for different plasma concentrations caused by varying platelet counts of individual donors and potential absorption of the drug by plasma proteins. For dynein inhibition, platelets were incubated with 1 mM EHNA (Sigma-Aldrich). For myosin II inhibition, we used (−)-blebbistatin (EMD Millipore), which was prepared as a 25-mM stock solution in DMSO and then diluted under vigorous agitation into PBS preheated to 45°C to avoid precipitation as previously described (Swift et al., 2012). The solution was then centrifuged before addition of platelets.

Immunofluorescence

Fixed platelets on coverslips were permeabilized with PBS/0.2% Triton X-100 for 15 min at RT and then incubated with blocking buffer (3% BSA and 10% goat serum in PBS) for 1 h at RT. Coverslips were then incubated for 2 h with primary antibodies diluted in blocking buffer and then washed twice with PBS and once with PBS/0.2% Triton X-100 and incubated with secondary antibodies diluted in blocking buffer for 2 h at RT. After three washing steps, coverslips were mounted on glass slides using Mowiol.

Image acquisition and processing

Fluorescent images were acquired and processed as follows for each figure. For Fig. 1 B and Fig. S1 A, a wide-field epifluorescence microscope (BX41; Olympus), objective Plan 100×/1.25 NA oil, camera (DP70; Olympus), and acquisition software (analySIS; Olympus) were used. For Fig. 1 C, a wide-field epifluorescence microscope (BX41), objective Plan 100×/1.25 NA oil, camera (DP70), and acquisition software (analySIS) were used. Merges were produced using Photoshop (Adobe). For Fig. 1 D, a confocal laser-scanning microscope (LSM 510; Carl Zeiss) objective Plan Apochromat 100×/1.4 NA oil, and acquisition software (LSM 510) were used. The 3D reconstitution was produced using MetaMorph (Molecular Devices). For Fig. 2 A, a confocal laser-scanning microscope (LSM 510), objective Plan Apochromat 100×/1.4 NA oil, and acquisition software (LSM 510) were used. The 3D reconstitution was produced using ImageJ 3D Project (National Institutes of Health). For Fig. 2 B, Fig. 3 B, Fig. 5 A, and Fig. S2 A, a confocal laser-scanning microscope (LSM 710; Carl Zeiss), objective Plan Apochromat 63×/1.4 NA oil, and acquisition software (Zen 2010; Carl Zeiss) were used. Image processing was performed using the custom ImageJ macro Marginal Band 3D Analysis (Supplemental material), and the 3D reconstitution was performed with ImageJ 3D Project. For Fig. 2 C, a confocal laser-scanning microscope (LSM 510), objective Plan Apochromat 100×/1.4 NA oil differential interference contrast III, and acquisition software (LSM 510) were used. Image processing was performed with MetaMorph. For acquisition details, see the legend of Video 4. For Fig. 2 (D and E) and Fig. S2 B, a confocal laser-scanning microscope (LSM 710), objective Plan Apochromat 63×/1.4 NA oil, and acquisition software (Zen 2010) were used. 3D reconstitution and depth coding were performed using the custom ImageJ macro 3D Project Color Depth Coding (Supplemental material). For acquisition details, see the legends of Videos 5, 6, and 10. For Fig. 3 A, a confocal laser-scanning microscope (LSM 710), objective Plan Apochromat 63×/1.4 NA oil, and acquisition software (Zen 2010) were used. Image processing and 3D reconstitution were performed using the custom ImageJ macro Marginal Band 3D Analysis. For Fig. 4 (A–F), a confocal laser-scanning microscope (LSM 710), objective Plan Apochromat 63×/1.4 NA oil, and acquisition software (Zen 2010) were used. 3D reconstitutions in the top images were produced using ImageJ 3D Project, and skeletonization of MBs in the bottom images were obtained using the custom ImageJ macro Marginal Band 3D Analysis.

3D MB length measurements

The length of MBs was measured using the custom ImageJ macro Marginal Band 3D Analysis. In brief, after acquisition of confocal z stacks, the stacks were first interpolated using the processing software ImageJ to obtain isotropic voxels (Abramoff et al., 2004). Then, a band pass filter was applied using the difference of two Gaussian filters. With the first filter, the original stack was smoothed by convolving with a 3D Gaussian kernel of standard deviation s1. Using a second filter, the original stack was smoothed with a Gaussian kernel of standard deviation s2, with s2 < s1 (here, we used s1 = 7 and s2 = 2). The difference of Gaussians stack was computed from the difference of the two smoothed stacks. After thresholding, the platelet skeleton was obtained and measured with the ImageJ plugin AnalyzeSkeleton, which allows pruning and loop closing in a user-defined manner for each platelet (Arganda-Carreras et al., 2010).

Delivery of antibodies into living platelets

Antibodies were introduced into platelets using the protein delivery kit (Chariot; Active Motif). In brief, 2 µg antibodies in 50 µl PBS was incubated with 2 µl Chariot in 50 µl H_2O for 30 min at RT. 10^6 platelets in 100 µl PBS were then added to the antibody/Chariot mix and incubated for 1 h at RT to allow antibody internalization before being used in the spreading assay.

MB staining of living platelets

For the spreading assay, PRP (2 ml prepared from buffy coats) was centrifuged for 10 min, 900 *g*, at RT. The platelet pellet was resuspended in 1 ml PBS containing the reagent (taxol-based compound coupled to a fluorochrome; Tubulin Tracker) at a final concentration of 500 nM and incubated for 30 min at 37°C before time-lapse video microscopy. For suspension activations, platelets were diluted in PBS, 1.6×10^7/ml, and 1 µl tracker reagent was added per milliliter of platelet suspension. After 30–60 min of incubation at RT, the suspension was diluted with an equal volume of PBS, and 500 µl was pipetted into 4-well slides (Lab-Tek; Thermo Fisher Scientific). Platelets were imaged at RT and activated by the addition of one drop (36 µl) of agonist solution to obtain final concentrations as indicated.

Video microscopy

Imaging of spreading platelets by fluorescence and differential interference contrast was performed using the inverted confocal microscope (LSM 510) equipped with a 100×/1.4 Plan Apochromat objective. The pinhole was adjusted to 2 arbitrary units, and the confocal plane was positioned slightly above the glass surface. The fluorescence excitation at 488 nm was attenuated to 0.2% acousto-optic tunable filter transmission. Platelets were allowed to sediment on chambered coverslips (Lab-Tek) at RT. Images were acquired every 5 s.

3D confocal video microscopy was performed in single-photon detection mode with a confocal microscope (LSM 710 ConfoCor 3), 63×/1.4 NA Plan Apochromat objective, long pass 505-nm emission filter, and single-photon avalanche photodiode detector (ConfoCor 3). The 488-nm excitation power at the objective output was only 30 nW (0.005% acousto-optic tunable filter transmission), ensuring no fluorescence photobleaching throughout the whole time-lapse acquisition and no laser-induced platelet activation as compared with the nonirradiated zones at the end of the experiment. The pinhole was closed to 1 arbitrary unit, and the voxel size was set to 66 × 66 × 500 nm with a pixel dwell time of 6.3 µs. Six planes spaced by 0.5 µm were imaged in each z stack. Image processing and color depth coding were made with the custom ImageJ macro 3D Project Color Depth Coding.

Quantification

For all platelet quantification data, >50 platelets were analyzed per experiment after confocal z-stack acquisitions. Data are expressed in percentages as means ± SEM obtained from several individual experiments as indicated.

Online supplemental material

Fig. S1 shows the quantification of experiments presented in Fig. 1 (B and C) on the inhibition of microtubule motor proteins. Fig. S2 shows MB coiling induced by different concentrations of ADP after treatment of platelets with the dynein inhibitor, the Tubulin Tracker, or taxol and two time points of time-lapse videos of microtubule tracker-stained platelets with MB coiling induced by calyculin. Fig. S3 shows MB length measurements at successive time points during MB coiling shown in the time-lapse videos Video 5 after ADP activation and kinesin inhibition and Video 6 after ADP activation. Video 1 (Fig. 1 D) shows a 360° rotation of MBs induced to coil by kinesin inhibition. Video 2 (Fig. 2 A) shows a 360° rotation of acetylated, coiled MBs in transiently activated platelets. Video 3 (Fig. 2 B) shows a 360° rotation of coiled MBs in platelets activated by mechanical stress, arachidonic acid, ADP, or thrombin. Video 4 (Fig. 2 C) shows a time-lapse video of MB coiling during platelet spreading. Video 5 (Fig. 2 D) shows time-lapse videos of MB coiling triggered by thrombin, ADP, or kinesin inhibition. Video 6 (Fig. 2 E) shows a time-lapse video at two different view angles of MB coiling after platelet activation with ADP illustrating the coiling stage at which newly polymerized microtubules shortcut the coiled bundle. Video 7 (Fig. 3 B) shows a 360° rotation of MBs present in platelets prepared from freshly drawn blood with and without dynein inhibition. Video 8 (Fig. 4, A–C) shows a 360° rotation of platelets with resting

or slightly coiled MBs triple stained for acetylated, tyrosinated, and total tubulin as well as the same images reduced to one voxel skeletons. Video 9 (Fig. 4, D–F) shows a 360° rotation of platelets with strongly coiled MBs triple stained for acetylated, tyrosinated, and total tubulin as well as the same images reduced to one voxel skeletons. Video 10 (Fig S2 B) shows time-lapse videos of MB coiling induced by activation of actomyosin contraction. A source code for a custom ImageJ macro for Marginal Band 3D Analysis, with a toolset for image processing, 3D viewing, skeletonization of MBs, manual skeleton editing, and MB length measurements is provided online as a text file. A source code for a custom ImageJ macro for 3D Project Color Depth Coding, with a tool for depth color coding of 3D confocal time-lapse series and visualization at different view angles is provided online as a text file. Online supplemental material is available at http://www.jcb.org/cgi/content/full/jcb.201306085/DC1. Additional data are available in the JCB DataViewer at http://dx.doi.org/10.1083/jcb.201306085.dv.

We are grateful to Joel Plumas and Sandrine Fournel for access to buffy coats, Veronique Gerson and Liliane Chollez for blood sampling, Didier Job and Bertrand Fourcade for helpful discussions, and Richard Abbatt and Arthur Forer for critical reading of the manuscript. We acknowledge the assistance of Jacques Mazzega (Platform Optical microscopy–Cell Imaging, Centre de Recherche Institut National de la Santé et de la Recherche Médicale U823).

The microscopy equipment was supported by the Association for Research on Cancer, Ministère de l'Enseignement Supérieur et de la Recherche, and the Rhone-Alpes region (Contrat de projets État–Région Exploration du vivant, imagerie biomedicale), work by J. Wang was supported by a grant from the Science and Technology Commission of Shanghai Municipality (12410705400), and work in the S. Khochbin laboratory was supported by Agence Nationale de la Recherche and Institut National du Cancer grants.

Submitted: 14 June 2013
Accepted: 4 December 2013

References

Abramoff, M.D., P.J. Magalhaes, and S.J. Ram. 2004. Image Processing with ImageJ. *Biophotonics International*. 11:36–42.

Arganda-Carreras, I., R. Fernández-González, A. Muñoz-Barrutia, and C. Ortiz-De-Solorzano. 2010. 3D reconstruction of histological sections: Application to mammary gland tissue. *Microsc. Res. Tech.* 73:1019–1029. http://dx.doi.org/10.1002/jemt.20829

Aslan, J.E., K.G. Phillips, L.D. Healy, A. Itakura, J. Pang, and O.J. McCarty. 2013. Histone deacetylase 6-mediated deacetylation of α-tubulin coordinates cytoskeletal and signaling events during platelet activation. *Am. J. Physiol. Cell Physiol.* 305:C1230–C1239. http://dx.doi.org/10.1152/ajpcell.00053.2013

Behnke, O., and A. Forer. 1998. From megakaryocytes to platelets: platelet morphogenesis takes place in the bloodstream. *Eur. J. Haematol. Suppl.* 61:3–23.

Bull, B.S., and M.B. Zucker. 1965. Changes in platelet volume produced by temperature, metabolic inhibitors, and aggregating agents. *Proc. Soc. Exp. Biol. Med.* 120:296–301. http://dx.doi.org/10.3181/00379727-120-30516

Calaminus, S.D., J.M. Auger, O.J. McCarty, M.J. Wakelam, L.M. Machesky, and S.P. Watson. 2007. MyosinIIa contractility is required for maintenance of platelet structure during spreading on collagen and contributes to thrombus stability. *J. Thromb. Haemost.* 5:2136–2145. http://dx.doi.org/10.1111/j.1538-7836.2007.02696.x

Conrad, M., J. DeNobile, I. Chaikhoutdinov, D. Escribano, K.G. Lee, and W.D. Cohen. 2004. Cytoskeletal organization of limulus amebocytes pre- and post-activation: comparative aspects. *Biol. Bull.* 207:56–66. http://dx.doi.org/10.2307/1543628

Dompierre, J.P., J.D. Godin, B.C. Charrin, F.P. Cordelières, S.J. King, S. Humbert, and F. Saudou. 2007. Histone deacetylase 6 inhibition compensates for the transport deficit in Huntington's disease by increasing tubulin acetylation. *J. Neurosci.* 27:3571–3583. http://dx.doi.org/10.1523/JNEUROSCI.0037-07.2007

Duhl, D.M., and P.A. Renhowe. 2005. Inhibitors of kinesin motor proteins—research and clinical progress. *Curr. Opin. Drug Discov. Devel.* 8:431–436.

Grabham, P.W., G.E. Seale, M. Bennecib, D.J. Goldberg, and R.B. Vallee. 2007. Cytoplasmic dynein and LIS1 are required for microtubule advance during growth cone remodeling and fast axonal outgrowth. *J. Neurosci.* 27:5823–5834. http://dx.doi.org/10.1523/JNEUROSCI.1135-07.2007

Hartwig, J.H. 2006. The platelet: form and function. *Semin. Hematol.* 43(Suppl. 1): S94–S100. http://dx.doi.org/10.1053/j.seminhematol.2005.11.004

Janke, C., and J.C. Bulinski. 2011. Post-translational regulation of the microtubule cytoskeleton: mechanisms and functions. *Nat. Rev. Mol. Cell Biol.* 12:773–786. http://dx.doi.org/10.1038/nrm3227

Johnson, G.J., L.A. Leis, M.D. Krumwiede, and J.G. White. 2007. The critical role of myosin IIA in platelet internal contraction. *J. Thromb. Haemost.* 5:1516–1529. http://dx.doi.org/10.1111/j.1538-7836.2007.02611.x

Laan, L., S. Roth, and M. Dogterom. 2012. End-on microtubule-dynein interactions and pulling-based positioning of microtubule organizing centers. *Cell Cycle*. 11:3750–3757. http://dx.doi.org/10.4161/cc.21753

Lee, K.G., T. Miller, I. Anastassov, and W.D. Cohen. 2004. Shape transformation and cytoskeletal reorganization in activated non-mammalian thrombocytes. *Cell Biol. Int.* 28:299–310. http://dx.doi.org/10.1016/j.cellbi.2004.01.008

Lippi, G., L. Ippolito, V. Zobbi, F. Sandei, and E.J. Favaloro. 2013. Sample collection and platelet function testing: influence of vacuum or aspiration principle on PFA-100 test results. *Blood Coagul. Fibrinolysis*. 24:666–669. http://dx.doi.org/10.1097/MBC.0b013e32835fada7

Matsuyama, A., T. Shimazu, Y. Sumida, A. Saito, Y. Yoshimatsu, D. Seigneurin-Berny, H. Osada, Y. Komatsu, N. Nishino, S. Khochbin, et al. 2002. In vivo destabilization of dynamic microtubules by HDAC6-mediated deacetylation. *EMBO J.* 21:6820–6831. http://dx.doi.org/10.1093/emboj/cdf682

Patel, S.R., J.L. Richardson, H. Schulze, E. Kahle, N. Galjart, K. Drabek, R.A. Shivdasani, J.H. Hartwig, and J.E. Italiano Jr. 2005. Differential roles of microtubule assembly and sliding in proplatelet formation by megakaryocytes. *Blood*. 106:4076–4085. http://dx.doi.org/10.1182/blood-2005-06-2204

Patel-Hett, S., J.L. Richardson, H. Schulze, K. Drabek, N.A. Isaac, K. Hoffmeister, R.A. Shivdasani, J.C. Bulinski, N. Galjart, J.H. Hartwig, and J.E. Italiano Jr. 2008. Visualization of microtubule growth in living platelets reveals a dynamic marginal band with multiple microtubules. *Blood*. 111:4605–4616. http://dx.doi.org/10.1182/blood-2007-10-118844

Penningroth, S.M., A. Cheung, P. Bouchard, C. Gagnon, and C.W. Bardin. 1982. Dynein ATPase is inhibited selectively in vitro by erythro-9-[3-2-(hydroxynonyl)]adenine. *Biochem. Biophys. Res. Commun.* 104:234–240. http://dx.doi.org/10.1016/0006-291X(82)91964-7

Piperno, G., M. LeDizet, and X.J. Chang. 1987. Microtubules containing acetylated α-tubulin in mammalian cells in culture. *J. Cell Biol.* 104:289–302. http://dx.doi.org/10.1083/jcb.104.2.289

Reed, N.A., D. Cai, T.L. Blasius, G.T. Jih, E. Meyhofer, J. Gaertig, and K.J. Verhey. 2006. Microtubule acetylation promotes kinesin-1 binding and transport. *Curr. Biol.* 16:2166–2172. http://dx.doi.org/10.1016/j.cub.2006.09.014

Rothwell, S.W., and V.S. Calvert. 1997. Activation of human platelets causes post-translational modifications to cytoplasmic dynein. *Thromb. Haemost.* 78:910–918.

Sadoul, K., J. Wang, B. Diagouraga, A.L. Vitte, T. Buchou, T. Rossini, B. Polack, X. Xi, P. Matthias, and S. Khochbin. 2012. HDAC6 controls the kinetics of platelet activation. *Blood*. 120:4215–4218. http://dx.doi.org/10.1182/blood-2012-05-428011

Schatten, G., C. Simerly, D.J. Asai, E. Szöke, P. Cooke, and H. Schatten. 1988. Acetylated alpha-tubulin in microtubules during mouse fertilization and early development. *Dev. Biol.* 130:74–86. http://dx.doi.org/10.1016/0012-1606(88)90415-0

Severin, S., F. Gaits-Iacovoni, S. Allart, M.P. Gratacap, and B. Payrastre. 2013. A confocal-based morphometric analysis shows a functional crosstalk between the actin filament system and microtubules in thrombin-stimulated platelets. *J. Thromb. Haemost.* 11:183–186. http://dx.doi.org/10.1111/jth.12053

Swift, L.M., H. Asfour, N.G. Posnack, A. Arutunyan, M.W. Kay, and N. Sarvazyan. 2012. Properties of blebbistatin for cardiac optical mapping and other imaging applications. *Pflugers Arch.* 464:503–512. http://dx.doi.org/10.1007/s00424-012-1147-2

Theiss, C., M. Napirei, and K. Meller. 2005. Impairment of anterograde and retrograde neurofilament transport after anti-kinesin and anti-dynein antibody microinjection in chicken dorsal root ganglia. *Eur. J. Cell Biol.* 84:29–43. http://dx.doi.org/10.1016/j.ejcb.2004.09.001

Thon, J.N., H. Macleod, A.J. Begonja, J. Zhu, K.C. Lee, A. Mogilner, J.H. Hartwig, and J.E. Italiano Jr. 2012. Microtubule and cortical forces determine platelet size during vascular platelet production. *Nat Commun*. 3:852. http://dx.doi.org/10.1038/ncomms1838

Tolić-Nørrelykke, I.M. 2008. Push-me-pull-you: how microtubules organize the cell interior. *Eur. Biophys. J.* 37:1271–1278. http://dx.doi.org/10.1007/s00249-008-0321-0

White, J.G., and S.M. Burris. 1984. Morphometry of platelet internal contraction. *Am. J. Pathol.* 115:412–417.

White, J.G., and G.H. Rao. 1998. Microtubule coils versus the surface membrane cytoskeleton in maintenance and restoration of platelet discoid shape. *Am. J. Pathol.* 152:597–609.